Energetic analysis of succinic acid in water droplets: insight into the size-dependent solubility of atmospheric nanoparticles

Chuchu Chen[1,2], Xiaoxiang Wang[1,6], Kurt Binder[3], Mohammad Mehdi Ghahremanpour[4,5], David van der Spoel[4], Ulrich Pöschl[2], Hang Su[2], Yafang Cheng[1]

[1]Minerva Research Group, Max Planck Institute for Chemistry, Hahn-Meitner-Weg 1, 55128 Mainz, Germany
[2]Multiphase Chemistry Department, Max Planck Institute for Chemistry, Hahn-Meitner-Weg 1, 55128 Mainz, Germany
[3]Institute of Physics, Johannes Gutenberg University of Mainz, Staudinger Weg 7, 55128 Mainz, Germany
[4]Department of Cell and Molecular Biology, Uppsala University, Husargatan 3, Box 596, SE-75124 Uppsala, Sweden
[5]Department of Chemistry, Yale University, New Haven, CT 06520-8107, USA
[6]School of Environmental Science and Engineering, Southern University of Science and Technology, 518055 Shenzhen, P. R. China

Correspondence to: Yafang Cheng (yafang.cheng@mpic.de)

Abstract. Size-dependent solubility is prevalent in atmospheric nanoparticles, but a molecular level understanding is still insufficient, especially for organic compounds. Here, we performed molecular dynamics simulations to investigate the size dependence of succinic acid solvation on the scale of ~1-4 nm with the potential of mean forces method. Our analyses reveal that the surface preference of succinic acid is stronger for a droplet than the slab of the same size, and the surface propensity is enhanced due to the curvature effect as the droplet becomes smaller. Energetic analyses show that such surface preference is primarily an enthalpic effect in both systems, while the entropic effect further enhances the surface propensity in droplets. On the other hand, with decreasing droplet size, the solubility of succinic acid in the internal bulk volume may decrease, imposing an opposite effect on the size dependence of solubility as compared with the enhanced surface propensity. Meanwhile, structural analyses, however, show that the surface to internal bulk volume ratio increases drastically, especially when considering the surface in respect to succinic acid, e.g., for droplet with radius of 1 nm, the internal bulk volume would be already close to zero for the succinic acid molecule.

1 Introduction

Organic compositions in aerosol particles play a vital role in new particle formation and growth, as well as aerosol activation and chemical reactions in the atmosphere (Matsumoto et al., 1997; Riipinen et al., 2012; Metzger et al., 2010; Kirkby et al., 2011; Zhang et al., 2004; Kroll et al., 2011). Organic compositions participate in chemical and physical processes in the internal bulk volume (referred to as the bulk of confined volumes except surface volumes) as well as at the surface area of aerosol particles, and the reactions at the surface are evidenced to be unique compared to the reactions in the internal bulk volume (Finlayson-Pitts, 2009; Donaldson and Valsaraj, 2010; Hayase et al., 2011; Martins-Costa et al., 2012; Monge et al., 2012). However, the influence of organic compositions in the aerosol surface volume, such as the surface partitioning, adsorption

probabilities, and phase separation, is still not well understood experimentally and theoretically (Rudich, 2003; Donaldson and Vaida, 2006; Fuzzi et al., 2006; Rudich et al., 2007; Bluhm and Siegmann, 2009; Werner et al., 2016).

It has been found that particle size plays an important role in regulating the phase transition of atmospheric nanoparticles. Bulk
35 thermodynamics have shown that chemical composition, relative humidity, temperature, and pressure are the main factors controlling aerosol phase state, but they cannot fully explain the observed phenomenon for nanometer-sized particles (Biskos et al., 2006a; Biskos et al., 2006b; Virtanen et al., 2010; Krieger et al., 2012; You et al., 2012; Veghte et al., 2013; Cheng et al., 2015; Werner et al., 2016; Freedman, 2017). Several studies have demonstrated that the phase transitions of nanoparticles have significant size dependence. For instance, Biskos et al. (2006a) found that deliquescence and efflorescence occur at higher
40 relative humidity for sodium chloride nanoparticles using Humidified Tandem Differential Mobility Analyzer (HTDMA) experiments. And Cheng et al. (2015) developed Differential Köhler Analysis to explain the size dependence of deliquescence and efflorescence for the sodium chloride nanoparticles. The morphology of particles was also observed through experiments, where phase separation of aerosol particles is dependent on both particle size and components (You et al., 2012; Veghte et al., 2013; Cheng et al., 2015).

45 Size dependence of organic molecule solvation in the nanoparticles as one of the phase transitions has been suspected to be prevalent. Favorable surface solvation of organic molecules was known to enhance the solubility of solutes at the surface of the nanodroplet with molecular dynamics (MD) simulation by Hub et al. (2012). Similar results were shown in Sayou et al. (2017) and attractive and repulsive interactions of the organic solute with water molecules were analyzed to explain the surface propensity of organic molecules in the droplet. Besides, Werner et al. (2016) probed the surface activity of succinic acid in
50 sodium chloride and ammonium sulphate solutions by X-ray Photoelectron Spectroscopy (XPS) experiments. The result suggests that succinic acid has a higher solubility at the surface of bulk solutions compared with the total solubility of bulk solutions because of fewer water molecules for hydration at the surface. Furthermore, Werner et al. (2016) developed a partitioned particle model, where the surface region used the surface concentrations estimated from XPS experiments and the internal bulk volume had the bulk-like particle concentration, indicating that the size-dependent solubility of surface-active
55 organic molecules can further enhance cloud activation and chemical reactions in the atmosphere. Despite of the importance of the size dependence of organic molecule solvation, how the solubility in the internal bulk volume as well as at the surface part of nanodroplets changes, particularly with changing droplet size and the underlying driving mechanism is still unclear.

In this study, size dependence of organic composition solvation in the nanoparticles is investigated based on the molecular dynamics (MD) simulation and energetic analysis. Succinic acid is chosen as a surrogate in the simulation because it is present
60 in the atmospheric aerosol particles (Hyvärinen et al., 2006; Werner et al., 2014). The simulations are performed for one single succinic acid molecule in different sizes of water nanodroplets (i.e., droplet radius from ~1 nm to 4 nm) and different thickness of water planar slabs (i.e., half slab thickness from ~1 nm to 4 nm). We compare the potential of mean forces (PMFs) derived from the simulations, as well as the enthalpic and entropic components decomposed from PMFs, to identify the potential driving forces for the size dependence of succinic acid solvation and discuss the size dependence of succinic acid solubility.

2 Methods

2.1 PMF calculations

Potential of Mean Forces (PMFs), the free-energy profiles along the chosen coordinate (along the center of mass of water droplets or slabs to the air), were computed using the method of umbrella sampling with a weighted histogram analysis method (Kumar et al., 1995; Souaille and Roux, 2001; Hub et al., 2010). This method is based on the protocol described in Caleman et al. (2011) and Sayou et al. (2017).

The MD simulations were computed with GROMACS 2016.5 (Van Der Spoel et al., 2005; Abraham et al., 2015). The solute (succinic acid molecule) was treated with the Generalized Amber force field (GAFF) with the electrostatic potential (ESP) calculated charges (B3LYP/aug-cc-pVTZ). Although aerosol pH in the atmosphere may vary in a large range (Zheng et al., 2020), the majority of fine particles (diameter < 1 μm) is with pH below ~3-4 (Fig. 2 of Pye et al. (2020)). In this pH range, the form of succinic acid is more relevant as hydrogen-succinate and succinate dominate only at higher pH. Besides, recent study shows that the surface of pure water droplets and slabs is slightly enriched in hydronium, which might lead to some portion of succinic acid having a different protonation state in the internal bulk volume as on the surface as well (Hub et al., 2014), but the influence is not expected to be large to the aerosol pH. The solvent (water) was described with the TIP4P/2005 force field, as compared to four other water models the combination of TIP4P/2005 with above force field of succinic acid produce the closest hydration free energy (ΔG_{hyd}) of single succinic acid molecule to the experimental value (Fig. S1 and SI).

Newton's equation of motion was integrated with the leapfrog integration scheme at a time step of 2 fs (Van Gunsteren and Berendsen, 1988). The temperature was controlled at 298.15 K using the stochastic dynamics integrator at a coupling constant of 0.1 ps (Van Gunsteren and Berendsen, 1988). The covalent bonds to hydrogen atoms were fixed by Linear Constraint Solver (LINCS) algorithm (Miyamoto and Kollman, 1992; Hess et al., 1997).

The droplets without periodic boundary conditions were simulated as isolated systems (Fig. 1a). The simulations consisted of a single succinic acid molecule with 140, 1117, 3768, and 8932 water molecules, corresponding to aqueous droplets with approximate radius 1 nm, 2 nm, 3 nm and 4 nm, respectively. The center of mass of the water molecules was fixed at the origin, and no cutoffs were applied to any intermolecular interactions (Fig. 1a).

The umbrella potential was implemented as

$$F(r) = \frac{k(r - r_{\mathrm{c}})^2}{2} \tag{1}$$

where k was set to 1000 kJ mol^{-1} nm^{-2}, r is the radial distance of the solute center of mass from the center of mass of the water molecules. Along with the reaction coordinate r, 20 windows with r_{c} of 0, 0.2, …, 4 nm, 25 windows with r_{c} of 0, 0.2, …, 5 nm, 35 windows with r_{c} of 0, 0.2, …, 7 nm, and 35 windows with r_{c} of 0, 0.2, …, 7 nm were prepared for the droplet systems (i.e., droplet radius from ~1 nm to 4 nm). Since the simulations were performed at the room temperature, to prevent individual

95   water molecules from frequent evaporation from the droplet surface that may lead to an ill-defined droplet center of mass, a spherical flat-bottom restraining potential was applied to each water molecule. The potential was given by

$$V_{\text{fb}}(r) = \frac{1}{2} k_{\text{fb}} (r - r_{\text{fb}})^2 H(r - r_{\text{fb}}) \qquad (2)$$

where r is the radial distance of the oxygen atom of the water molecule from the center of mass of the water droplet, r_{fb} is the radius of the sphere around the center of mass without any additional force, which was taken to be 0.5 nm larger than the radius

100   of the water droplet. The force constant k_{fb} was set to 1000 kJ mol^{-1} nm^{-2}, and H is the Heaviside step function. The energy of each structure was minimized, and the umbrella sampling was then conducted for 51 ns for each window of the solute location.

After removing the first 1 ns of each trajectory for equilibration, the PMFs for droplet systems were computed by the integration of the mean force. An analytical entropy correction for the PMFs of the droplet systems (Neumann, 1980) was computed as

$$\Delta S(r) = 2 k_{\text{B}} \ln(r) \qquad (3)$$

105   where k_{B} is the Boltzmann factor, r is the radial distance of the solute center of mass from the center of mass of the water molecules. This correction is due to the fact that for the case when the succinic acid molecule is at a distance r, it can be anywhere in the volume of a spherical shell of size $4 \pi r^2 \Delta r$ (where $\Delta r = 0.2$ is the thickness of the shell) and hence the associated entropy, which scales as the logarithm of the volume of this shell times Boltzmann's constant, yields a term as written in Eq. (3).

110   The slab systems were simulated under the periodic boundary condition in x, y, z directions with the canonical (NVT) ensemble. The single succinic acid molecule was solvated in the center of rectangular water box with edge lengths of 3 nm to the x and y directions and of 2, 4, 6 and 8 nm to the z direction. The slab systems (Fig. 1b) consisted of 560, 1200, 1800, and 2400 water molecules, which correspond to 1, 2, 3, and 4 nm of half slab thickness, respectively. The systems were then elongated to 30 nm in the z direction to create liquid-vapor interfaces. The smooth particle-mesh Ewald (PME) method with a real-space cutoff

115   of 1.35 nm, a spline order of 6, and relative tolerance of 10^{-5} was used to the Coulombic interactions. The PME with a real-space cutoff of 1.35 nm was also used for the van der Waals interactions. The umbrella potential was implemented as

$$F(z) = \frac{k(z - z_{\text{c}})^2}{2} \qquad (4)$$

where k was set to 1000 kJ mol^{-1} nm^{-2}, z is the distance along the z direction of the solute center of mass from the center of mass of the water molecules. Along with the reaction coordinate z, 20 windows with z_{c} of 0, 0.2, …, 4 nm, 25 windows with

120   z_{c} of 0, 0.2, …, 5 nm, 35 windows with z_{c} of 0, 0.2, …, 7 nm, 35 windows with z_{c} of 0, 0.2, …, 7 nm were prepared for the slab systems (i.e., half slab thickness from ~1 nm to 4 nm). The center of mass of the water molecules was fixed at the center of the rectangular cell, and restraint was used to prevent possible water evaporation. The restraint was given by

$$V_{\text{fb}}(z) = \frac{1}{2} k_{\text{fb}} (z - z_{\text{fb}})^2 H(z - z_{\text{fb}}) \tag{5}$$

where z is the distance along the z direction of the oxygen atom of the water molecule from the cell center. z_{fb} was taken to be

125   0.5 nm larger than the half of thickness of the slab in the z direction. The force constant k_{fb} was set to 1000 kJ mol^{-1} nm^{-2}.

Figure 1c depicts the schematic free energy profiles of a succinic acid along the radius in the droplet system and along the z-axis in the slab system. As the molecule moves from the center of mass of water toward the gas phase, its free energy goes through a minimum at the water-vapor interface, then increases again, and finally reaches a plateau in the gas phase. The free energy difference of the transition of the solute from the gas to the internal bulk volume of liquid, ΔG_{ba}, represents the free

130   energy of hydration of succinic acid (Sayou et al., 2017). ΔG_{sb} is the free energy of the transition from the internal bulk volume to the liquid-vapor interface, and ΔG_{sa} is the free energy of the transition from the gas phase into the liquid-vapor interface.

To separate the energetic contributions that govern surface propensity, the PMFs of droplet systems and slab systems were further decomposed into enthalpic and entropic components. Under the canonical (NVT) ensemble, the enthalpic part ΔH was computed as the average potential energy of the system in each simulation. The entropic component was computed as

135
$$-T\Delta S = \Delta G - \Delta H \tag{6}$$

ΔH was further decomposed into water-water and solvent-water interactions in each system.

2.2 Structural analysis

For structural analysis, the water density profiles were calculated along the radius for the droplet systems and along the z-direction for the slab systems. For droplet, the simulation cell was divided into multiple shells with a thickness of 0.02 nm,

140   and the density of each shell was statistically calculated based on the cumulative radial distribution functions of water molecules. For slab, the simulation cell was divided into multiple slices with a thickness of 0.02 nm, and the density of each slice was statistically averaged over the simulation time. Both water density profiles from droplets and slabs were further fitted to a hyperbolic tangent function (Vega and de Miguel, 2007) as

$$\rho(s) = \frac{1}{2}(\rho_{\text{L}} + \rho_{\text{V}}) - \frac{1}{2}(\rho_{\text{L}} - \rho_{\text{V}}) \tanh\left[\frac{s - s_0}{t}\right] \tag{7}$$

145   where ρ_{L} and ρ_{V} are densities of water and vapor, s_0 is the position of the Gibbs-dividing surface, and t is a parameter about surface thickness.

3 Results and discussion

3.1 Size dependence of surface propensity

In Fig. 2, the calculated potential of mean forces (PMFs) profiles show a significant surface propensity of succinic acid in the
150 liquid phase with a minimum at the surface region for both water droplet and slab systems at all sizes. It indicates that the
succinic acid is more preferably located at the surface region than inside the internal bulk volume and the gas phase.

We further calculated the differences of free energy between succinic acid in the internal bulk volume, surface and air to
identify the size dependence of surface propensity of succinic acid. As shown in Fig. 3a, ΔG_{sb}, the free energy difference of
the transition of succinic acid from the internal bulk volume to the surface, is negative in every droplet and slab system,
155 reflecting the surface active of succinic acid. ΔG_{sb} in the droplet system is smaller than that in the slab system of the same size,
suggesting that the surface propensity in the droplet system is more enhanced than that in the slab system due to the curvature
effect. Similar results were observed in Sayou et al. (2017), where for ethane, benzene, methanol, and H_2S, curvature
dependence is appreciable and the magnitude is mainly related to the structure of organic molecules. Hub et al. (2012) also
supported this view in their study. Besides, based on XPS experiments, Werner et al. (2016) found the enrichment of surface
160 partitioning of succinic acid at the surface region of the bulk solutions.

Meanwhile, ΔG_{sa}, the free energy difference of the transition of succinic acid from gas to the water surface, which is negative
as well, is larger in the droplet system than that in the slab system of the same size (Fig. 3b), showing that the propensity of
succinic acid at the surface layer (relative to the gas phase) in the droplet system is less than that in the slab system.
Furthermore, the magnitude of the propensity is affected by the nature of the organic molecules as well as the temperature
165 (Sayou et al., 2017). As a result, the decrease of ΔG_{sb} and increase of ΔG_{sa} from slab to droplet with the uniform size indicates
that succinic acid is "pushed" from the internal bulk volume to the surface region more strongly but "pushed" from the air to
the surface region more slightly for the droplet systems. These two opposite forces further affect succinic acid to prefer to be
exposed more to the air in the droplet rather than in the slab, which further demonstrates that the droplet curvature enhances
the surface propensity of succinic acid.

170 When we compare the slab systems of different thicknesses, both ΔG_{sb} (Fig. 3a, blue circles) and ΔG_{sa} (Fig. 3b, blue triangles)
are almost constant with the increase of the thickness, suggesting a near constant surface propensity. In other words, the change
of slab thickness only has a very slight effect on the surface propensity of succinic acid. This is different from the results of
nanodroplet with a curvature/Kelvin effect. Without a curvature, the pressure inside the slab does not depend on the slab
thickness leading to almost unchanged surface propensity. And at the considered temperature, this pressure to very good
175 approximation is zero. However, for the droplet systems, when the radius of the droplet increases but the curvature of the
droplet decreases at the same time, ΔG_{sb} decreases first from radius 1 nm to 3 nm but then increases (Fig. 3a, orange circles),
showing that the surface propensity relative to the internal bulk volume is enhanced first and then weaken. ΔG_{sa} shows a
similar trend (Fig. 3b, orange triangles), meaning that the surface propensity relative to the air is also enhanced first and then

weakened. Overall, the surface propensity is weakened as the droplet becomes larger and the difference between the droplet

180   and slab systems becomes smaller when the droplet size increases. This result shows that different from thin slabs: for a nano-sized droplet, due to the Kelvin equation, the pressure inside the droplet is enhanced when the droplet size decreases.

3.2 Energetic analysis

To separate the energetic contributions that govern surface propensity of succinic acid, we decompose the PMF into the enthalpic and entropic components for both droplet systems (radius from ~1 nm to 3 nm) and slab systems (half thickness from

185   ~1 nm to 3 nm) (Fig. 4). Energetic decomposition for larger droplets and slabs is excluded due to the large uncertainties in the enthalpic component. Enthalpic curves are further divided into succinic acid-water interactions and water-water interactions (Fig. 5). For both droplet and slab systems, enthalpies show a significant minimum at the surface, demonstrating that the surface preference of succinic acid in both systems is primarily an enthalpic effect. However, the enthalpic minimum at the surface is partially compensated by the entropy, indicating that the entropy affects the magnitude of surface preference of

190   succinic acid.

On the contrary, the enthalpies show an increase in both droplets and slabs when being ~0.5 nm away from the surface, which may be caused by a reduced number of water-water interactions (Fig. 5, lines with open triangles). However, this increase of enthalpy is offset partially by the decreased entropy due to the increased rotational freedom of water molecules (Hub et al., 2012), resulting in a slight jump in the internal PMFs close to the surface. Furthermore, this jump becomes more significant

195   when the size of the droplet decreases, showing that enthalpy plays a more important role in that region when the droplet size decreases. In addition, enthalpy plays a leading role in the performance of the succinic acid molecule in the internal bulk volume of droplets as well as in the internal bulk volume of slabs. However, the internal enthalpy and entropy inside droplets fluctuate more intensely than those in the slab systems due to the more active molecule interactions (Fig. 5).

3.3 Discussion on size dependence of solubility

200   With XPS detected surface enrichment, Werner et al. (2016) predicted a higher solubility of succinic acid in the small nanodroplet, based on the speculative assumptions that (1) with decreasing droplet size, the thickness of surface is assumed to be constant of ~0.4 nm, a value determined as the full width at half maximum of carbon profile peak with MD simulation in a slab system ($3.9 \times 3.9 \times 3.9$ nm^3 succinic acid aqueous solution in a $3.9 \times 3.9 \times 13$ nm^3 slab, simulated for 1ns at 278.15 K) (Werner et al., 2014); (2) the surface region of the nanodroplet was supposed to have the same enhanced surface concentration of

205   succinic acid in the bulk solutions; and (3) the internal bulk volume of the nanodroplet was recognized to have the same solubility of succinic acid as that in the internal bulk volume of bulk solutions. With our results, we may revisit these assumptions and gain more insight into the size dependence of solvation of succinic acid in nanodroplets compared to slab systems.

The free energy of hydration (ΔG_{ba}) gives implications on the size dependence of solubility of succinic acid (Fig. 3c). As
210   shown in Fig. S1, the free energy of hydration of succinic acid in bulk solutions ΔG_{hyd} is -44.94 ± 1.4 kJ mol^{-1} by TI method
calculation based on the GAFF/ESP force field for succinic acid and the TIP4P/2005 force field for water molecules (SI). For
slab systems, ΔG_{ba} increases very slightly along with the increase of the slab thickness but not beyond the range of ΔG_{hyd} (Fig.
3c, pink block). It means that the potential of succinic acid hydration into the slab systems is basically unchanged no matter
how the slab thickness changes. This further indicates that the solubility of succinic acid in the internal bulk volume as well as
215   at the surface region of the slab systems is almost constant.

Interestingly, for droplet systems, the hydration free energy ΔG_{ba}, under the interactions of ΔG_{sb} and ΔG_{sa} by the curvature
effect, are significantly larger than ΔG_{hyd} at all sizes. The unfavorable succinic acid solvation in the internal bulk volume of
the nanodroplets decreases the solubility of succinic acid in the internal bulk volume of the nanodroplet compared to the
solubility in the internal bulk volume of the slabs. Furthermore, the hydration free energy is larger in the internal bulk volume
220   of small droplets than that in large ones, suggesting a decrease of succinic acid solubility in the internal bulk volume of
nanodroplet when the droplet size becomes smaller.

Although a larger hydration free energy usually suggests a smaller solubility in water, i.e., a decrease of succinic acid solubility
in the internal bulk volume of nanodroplet when the droplet size becomes smaller, the favorable surface solvation of succinic
acid enhances the surface solubility of succinic acid in the nanodroplets. Therefore, the overall size dependence of succinic
225   acid solubility with decreasing sizes of the nanodroplets is controlled by the competition between these two effects (i.e.,
decreased solubility in the internal bulk volume and increased surface enrichment) as well as the drastic change of surface to
internal bulk volume ratio.

To examine how the surface thickness and surface to internal bulk volume would change when the size of the systems
decreases, we calculated the water density profiles (Fig. 2, dash lines) fitted by the hyperbolic tangent function (Vega and de
230   Miguel, 2007; Wang et al., 2019) based on the distributions of water density from MD simulations (Fig. 2, open circles). The
surface thicknesses of different sizes of nanodroplets and slabs can then be obtained (Fig. 6a). It should be noted that the
surface thickness of the slab profiles systematically depends on the lateral linear dimension of the slab, which is 3 nm here.
Due to the capillary wave broadening it diverges logarithmically with this linear dimension, while in contrast, no such
ambiguity occurs for the surface thickness of droplets (Wang et al., 2019). The structural analyses show that the surface to
235   internal bulk volume ratio in water droplet increases significantly with decreasing droplet size (Fig. 6c), although the surface
thickness of water decreases at the same time. When droplet radius changes from 4 nm to 1 nm The water surface thickness
slightly decreases from ~0.34 nm to ~0.25 nm (Fig. 6a). This result is consistent with the previous researches involving
nanodroplets and slab water (Thompson et al., 1984; Ismail et al., 2006; Vega and de Miguel, 2007; Wang et al., 2019).

However, how to define the surface is another important issue here. Regarding succinic acid molecule, thermodynamic analysis
240   shows that when the droplet is smaller, enthalpy and entropy ranges in the internal bulk volume become narrower. As shown

in Fig. 5, for droplets of all sizes, the interaction of succinic acid molecule and water molecules shows a significant increase in both droplets and slabs when being ~1 nm away from the surface, indicating the surface thickness is effectively ~1 nm in respect to succinic acid molecule and is independent to the change of droplet size. Moreover, relatively stable interactions exist in the internal bulk volume of droplets with radius of 2 nm (Fig. 5b) and 3 nm (Fig. 5c), but not in the droplet with radius of 1 nm (Fig 5a). In this regard, for droplet with radius of 1 nm, the internal bulk volume is close to zero for succinic acid molecule, but in terms of water molecule, the radius of internal bulk volume is still ~0.75 nm (Fig. 6b). Thus, in respect to succinic acid molecule, the surface to internal bulk volume ratio would increase much stronger than that for water molecule. These results suggest that the width of the PMF profiles is not simply controlled by the width of the interface, what also matter is the effective range of intermolecular forces between the succinic acid molecule and the water molecules. Since these forces contain long-range contributions, it is understandable that a saturation of the PMF profiles in the center of the droplet or slab in Fig. 2 (at the same horizontal plateau) is not observed, unlike the behavior of the density profiles.

4 Conclusion

In conclusion, the size dependence of succinic acid solvation was probed based on the MD simulations and energetic analysis. The simulations were conducted for a single succinic acid molecule in the different sizes of water nanodroplets (i.e., droplet radius from ~1 nm to 4 nm) and different thickness of water planar slabs (i.e., half slab thickness from ~1 nm to 4 nm). On the one hand, energetic analyses reveal a stronger surface preference for a droplet than the slab of the same size, and the surface propensity is enhanced due to the curvature effect as the droplet becomes smaller. The energetic driving force underlying such surface preference is primarily an enthalpic effect in both systems, while the entropic effect further enhances the surface propensity in droplets. On the other hand, the energetic analyses gives implications on the size dependence of solubility of succinic acid in nanodroplets. The solubility of succinic acid in the internal bulk volume may decrease when the droplet becomes smaller, imposing an opposite effect on the size dependence of solubility as compared with the enhanced surface propensity. Meanwhile, the overall size dependence of succinic acid solubility is also controlled by the drastic change of surface to internal bulk volume ratio. However, structural analyses show that the surface to internal bulk volume ratio increases drastically, especially when considering the surface in respect to succinic acid, e.g., for droplet with radius of 1 nm, the internal bulk volume would be already close to zero for the succinic acid molecule.

Data availability

Readers who are interested in the data should contact the authors: Yafang Cheng (yafang.cheng@mpic.de), or Chuchu Chen (c.chen@mpic.de).

Supporting Information

270   The supporting information is available free of charge on the website.

Author contributions

Y.C. and H.S. conceived and led the study. C.C. performed the MD simulation and analyzed the data. D.S. and M.G provided the force field of succinic acid. C.C., Y.C., K.B., H.S., and X.W. interpreted the results. K.B., U.P., D.S., and M.G. discussed the results and commented on the manuscript. C.C., Y.C., and H.S. wrote the manuscript with inputs from all coauthors.

275   **Competing interests**

The authors declare no competing financial interest.

Acknowledgement

This work is supported by the Max Planck Society (MPG). Y. C. acknowledges the Minerva Program of MPG. X. W. acknowledges the Program of 2017ZT07Z479.

280

References

Abraham, M. J., Murtola, T., Schulz, R., Páll, S., Smith, J. C., Hess, B., and Lindahl, E.: GROMACS: High performance molecular simulations through multi-level parallelism from laptops to supercomputers, SoftwareX, 1, 19-25, 2015.

Biskos, G., Malinowski, A., Russell, L. M., Buseck, P. R., and Martin, S. T.: Nanosize Effect on the Deliquescence and the Efflorescence
285   of Sodium Chloride Particles, Aerosol Science and Technology, 40, 97-106, 10.1080/02786820500484396, 2006a.

Biskos, G., Paulsen, D., Russell, L., Buseck, P., and Martin, S.: Prompt deliquescence and efflorescence of aerosol nanoparticles, 2006b.

Bluhm, H., and Siegmann, H.: Surface science with aerosols, Surface science, 603, 1969-1978, 2009.

Caleman, C., Hub, J. S., van Maaren, P. J., and van der Spoel, D.: Atomistic simulation of ion solvation in water explains surface preference of halides, Proceedings of the National Academy of Sciences, 2011.

290   Cheng, Y., Su, H., Koop, T., Mikhailov, E., and Poschl, U.: Size dependence of phase transitions in aerosol nanoparticles, Nat Commun, 6, 5923, 10.1038/ncomms6923, 2015.

Donaldson, D., and Vaida, V.: The influence of organic films at the air− aqueous boundary on atmospheric processes, Chemical reviews, 106, 1445-1461, 2006.

Donaldson, D., and Valsaraj, K. T.: Adsorption and reaction of trace gas-phase organic compounds on atmospheric water film surfaces: A
295   critical review, Environmental science & technology, 44, 865-873, 2010.

Finlayson-Pitts, B. J.: Reactions at surfaces in the atmosphere: integration of experiments and theory as necessary (but not necessarily sufficient) for predicting the physical chemistry of aerosols, Physical Chemistry Chemical Physics, 11, 7760-7779, 2009.

Freedman, M. A.: Phase separation in organic aerosol, Chemical Society Reviews, 46, 7694-7705, 2017.

Fuzzi, S., Andreae, M., Huebert, B., Kulmala, M., Bond, T. C., Boy, M., Doherty, S., Guenther, A., Kanakidou, M., and Kawamura, K.:

300   Critical assessment of the current state of scientific knowledge, terminology, and research needs concerning the role of organic aerosols in the atmosphere, climate, and global change, Atmospheric Chemistry and Physics, 6, 2017-2038, 2006.

Hayase, S., Yabushita, A., Kawasaki, M., Enami, S., Hoffmann, M. R., and Colussi, A. J.: Weak acids enhance halogen activation on atmospheric water's surfaces, The Journal of Physical Chemistry A, 115, 4935-4940, 2011.

Hess, B., Bekker, H., Berendsen, H. J., and Fraaije, J. G.: LINCS: a linear constraint solver for molecular simulations, Journal of

305   computational chemistry, 18, 1463-1472, 1997.

Hub, J. S., De Groot, B. L., and Van Der Spoel, D.: g_wham□ A Free Weighted Histogram Analysis Implementation Including Robust Error and Autocorrelation Estimates, Journal of chemical theory and computation, 6, 3713-3720, 2010.

Hub, J. S., Caleman, C., and van der Spoel, D.: Organic molecules on the surface of water droplets--an energetic perspective, Phys Chem Chem Phys, 14, 9537-9545, 10.1039/c2cp40483d, 2012.

310   Hub, J. S., Wolf, M. G., Caleman, C., van Maaren, P. J., Groenhof, G., and van der Spoel, D.: Thermodynamics of hydronium and hydroxide surface solvation, Chemical Science, 5, 10.1039/c3sc52862f, 2014.

Hyvärinen, A.-P., Lihavainen, H., Gaman, A., Vairila, L., Ojala, H., Kulmala, M., and Viisanen, Y.: Surface Tensions and Densities of Oxalic, Malonic, Succinic, Maleic, Malic, andcis-Pinonic Acids, Journal of Chemical & Engineering Data, 51, 255-260, 10.1021/je050366x, 2006.

315   Ismail, A. E., Grest, G. S., and Stevens, M. J.: Capillary waves at the liquid-vapor interface and the surface tension of water, The Journal of chemical physics, 125, 014702, 2006.

Kirkby, J., Curtius, J., Almeida, J., Dunne, E., Duplissy, J., Ehrhart, S., Franchin, A., Gagné, S., Ickes, L., and Kürten, A.: Role of sulphuric acid, ammonia and galactic cosmic rays in atmospheric aerosol nucleation, Nature, 476, 429-433, 2011.

Krieger, U. K., Marcolli, C., and Reid, J. P.: Exploring the complexity of aerosol particle properties and processes using single particle

320   techniques, Chemical Society Reviews, 41, 6631-6662, 2012.

Kroll, J. H., Donahue, N. M., Jimenez, J. L., Kessler, S. H., Canagaratna, M. R., Wilson, K. R., Altieri, K. E., Mazzoleni, L. R., Wozniak, A. S., and Bluhm, H.: Carbon oxidation state as a metric for describing the chemistry of atmospheric organic aerosol, Nature Chemistry, 3, 133-139, 2011.

Kumar, S., Rosenberg, J. M., Bouzida, D., Swendsen, R. H., and Kollman, P. A.: Multidimensional free-energy calculations using the

325   weighted histogram analysis method, Journal of Computational Chemistry, 16, 1339-1350, 1995.

Martins-Costa, M. T., Anglada, J. M., Francisco, J. S., and Ruiz-Lopez, M. F.: Reactivity of atmospherically relevant small radicals at the air–water interface, Angewandte Chemie International Edition, 51, 5413-5417, 2012.

Matsumoto, K., Tanaka, H., Nagao, I., and Ishizaka, Y.: Contribution of particulate sulfate and organic carbon to cloud condensation nuclei in the marine atmosphere, Geophysical Research Letters, 24, 655-658, 1997.

330   Metzger, A., Verheggen, B., Dommen, J., Duplissy, J., Prevot, A. S., Weingartner, E., Riipinen, I., Kulmala, M., Spracklen, D. V., and Carslaw, K. S.: Evidence for the role of organics in aerosol particle formation under atmospheric conditions, Proceedings of the National Academy of Sciences, 107, 6646-6651, 2010.

Miyamoto, S., and Kollman, P. A.: Settle: An analytical version of the SHAKE and RATTLE algorithm for rigid water models, Journal of computational chemistry, 13, 952-962, 1992.

335   Monge, M. E., Rosenørn, T., Favez, O., Müller, M., Adler, G., Riziq, A. A., Rudich, Y., Herrmann, H., George, C., and D'Anna, B.: Alternative pathway for atmospheric particles growth, Proceedings of the National Academy of Sciences, 109, 6840-6844, 2012.

Neumann, R. M.: Entropic approach to Brownian movement, American Journal of Physics, 48, 354-357, 1980.

Pye, H. O., Nenes, A., Alexander, B., Ault, A. P., Barth, M. C., Clegg, S. L., Collett Jr, J. L., Fahey, K. M., Hennigan, C. J., and Herrmann, H.: The acidity of atmospheric particles and clouds, Atmospheric Chemistry and Physics, 20, 4809-4888, 2020.

340   Riipinen, I., Yli-Juuti, T., Pierce, J. R., Petäjä, T., Worsnop, D. R., Kulmala, M., and Donahue, N. M.: The contribution of organics to atmospheric nanoparticle growth, Nature Geoscience, 5, 453-458, 10.1038/ngeo1499, 2012.

Rudich, Y.: Laboratory perspectives on the chemical transformations of organic matter in atmospheric particles, Chemical Reviews, 103, 5097-5124, 2003.

Rudich, Y., Donahue, N. M., and Mentel, T. F.: Aging of organic aerosol: Bridging the gap between laboratory and field studies, Annu. Rev.
345   Phys. Chem., 58, 321-352, 2007.

Sayou, M., Ishizuka, R., and Matubayasi, N.: Energetic Analysis of Adsorption and Absorption of Small Molecule to Nanodroplet of Water, The Journal of Physical Chemistry B, 121, 5995-6001, 2017.

Souaille, M., and Roux, B.: Extension to the weighted histogram analysis method: combining umbrella sampling with free energy calculations, Computer physics communications, 135, 40-57, 2001.

350   Thompson, S., Gubbins, K., Walton, J., Chantry, R., and Rowlinson, J.: A molecular dynamics study of liquid drops, The Journal of chemical physics, 81, 530-542, 1984.

Van Der Spoel, D., Lindahl, E., Hess, B., Groenhof, G., Mark, A. E., and Berendsen, H. J.: GROMACS: fast, flexible, and free, Journal of computational chemistry, 26, 1701-1718, 2005.

Van Gunsteren, W. F., and Berendsen, H. J.: A leap-frog algorithm for stochastic dynamics, Molecular Simulation, 1, 173-185, 1988.

355   Vega, C., and de Miguel, E.: Surface tension of the most popular models of water by using the test-area simulation method, J Chem Phys, 126, 154707, 10.1063/1.2715577, 2007.

Veghte, D. P., Altaf, M. B., and Freedman, M. A.: Size dependence of the structure of organic aerosol, Journal of the American Chemical Society, 135, 16046-16049, 2013.

Virtanen, A., Joutsensaari, J., Koop, T., Kannosto, J., Yli-Pirilä, P., Leskinen, J., Mäkelä, J. M., Holopainen, J. K., Pöschl, U., and Kulmala,
360   M.: An amorphous solid state of biogenic secondary organic aerosol particles, Nature, 467, 824-827, 2010.

Wang, X., Binder, K., Chen, C., Koop, T., Pöschl, U., Su, H., and Cheng, Y.: Second inflection point of water surface tension in the deeply supercooled regime revealed by entropy anomaly and surface structure using molecular dynamics simulations, Physical Chemistry Chemical Physics, 21, 3360-3369, 2019.

Werner, J., Julin, J., Dalirian, M., Prisle, N. L., Öhrwall, G., Persson, I., Björneholm, O., and Riipinen, I.: Succinic acid in aqueous solution:
365   connecting microscopic surface composition and macroscopic surface tension, Physical Chemistry Chemical Physics, 16, 21486-21495, 2014.

Werner, J., Dalirian, M., Walz, M.-M., Ekholm, V., Wideqvist, U., Lowe, S. J., Öhrwall, G., Persson, I., Riipinen, I., and Björneholm, O.: Surface partitioning in organic–inorganic mixtures contributes to the size-dependence of the phase-state of atmospheric nanoparticles, Environmental science & technology, 50, 7434-7442, 2016.

370   You, Y., Renbaum-Wolff, L., Carreras-Sospedra, M., Hanna, S. J., Hiranuma, N., Kamal, S., Smith, M. L., Zhang, X., Weber, R. J., and
Shilling, J. E.: Images reveal that atmospheric particles can undergo liquid–liquid phase separations, Proceedings of the National
Academy of Sciences, 109, 13188-13193, 2012.

Zhang, R., Suh, I., Zhao, J., Zhang, D., Fortner, E. C., Tie, X., Molina, L. T., and Molina, M. J.: Atmospheric new particle formation
enhanced by organic acids, Science, 304, 1487-1490, 2004.

375   Zheng, G., Su, H., Wang, S., Andreae, M. O., Pöschl, U., and Cheng, Y.: Multiphase buffer theory explains contrasts in atmospheric aerosol
acidity, Science, 369, 1374-1377, 2020.

380

Figures
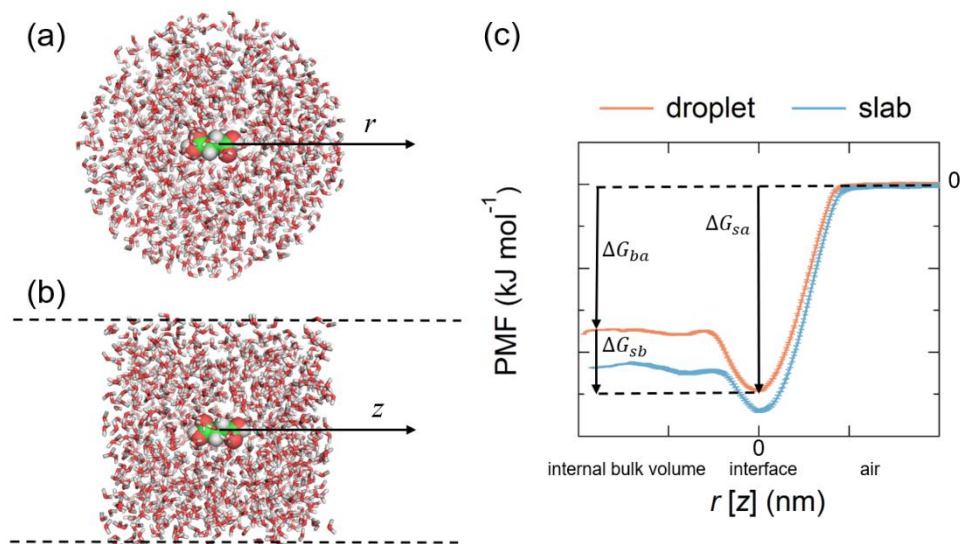
Figure 1: Model configuration and PMF calculations for water droplet and slab. Snapshot of the molecular configuration from the computation of the free energy profile of a succinic acid molecule coordinate across a liquid water droplet (a) and a liquid water slab (b). The succinic acid molecule is at the center of mass of the water droplet. (c) Typical PMF profiles of a succinic acid molecule in droplet and slab systems. The coordinate $r[z]$ is expressed in terms of the radical distance [distance along the z direction]. $r[z] = 0$ is where the PMF is minimum at the interface. ΔG_{ba}, ΔG_{sb}, and ΔG_{sa} are the free energy differences of the transition of the solute from the gas to the internal bulk volume of liquid, the internal bulk volume to the liquid-vapor interface, and the gas phase into the liquid-vapor interface, respectively.

385
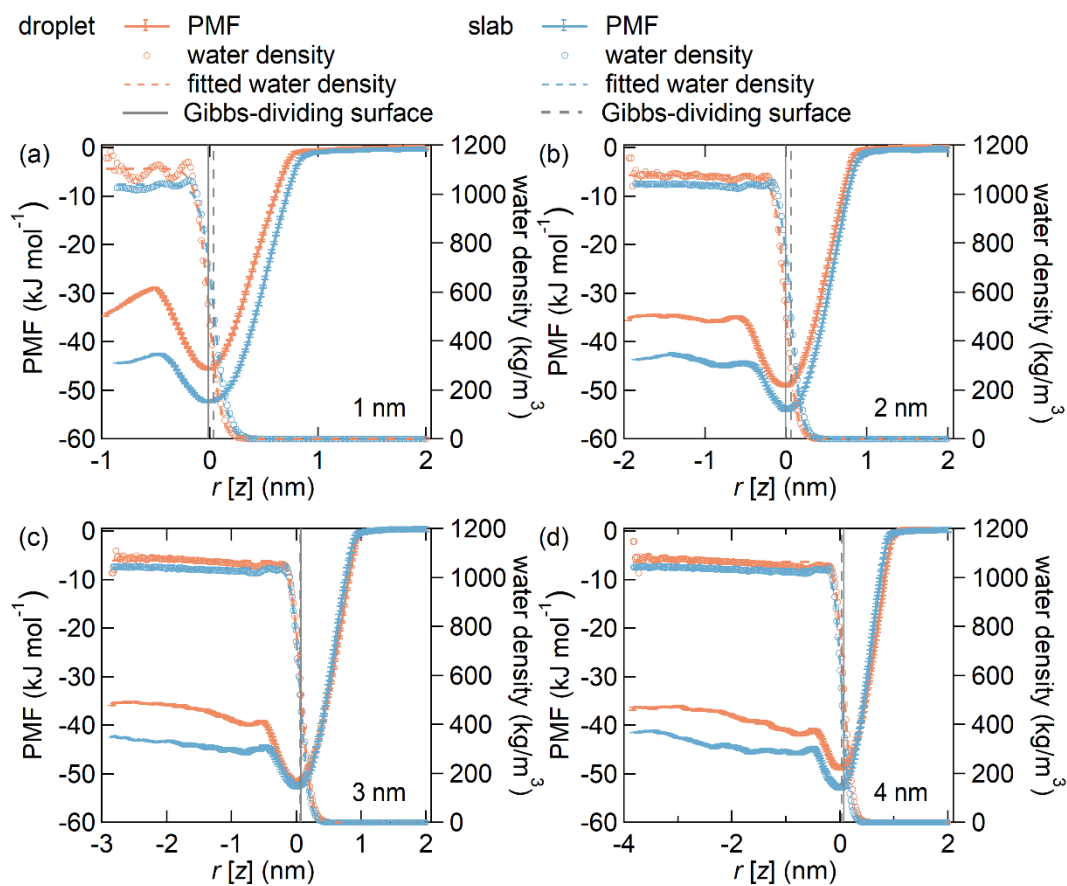
390

Figure 2: The potential of mean forces (PMFs) for succinic acid and density profiles of water in different sizes of droplet and slab systems at 298.15 K. All PMFs are defined to be zero outside of the droplets or slabs and thus quantify the free energy difference with respect to the internal bulk volume of water. The coordinate $r[z]$ is expressed in terms of the radial distance [distance along the z direction]. $r[z] = 0$ is where the PMF is minimum at the interface. The statistical errors are computed by binning analysis.

395
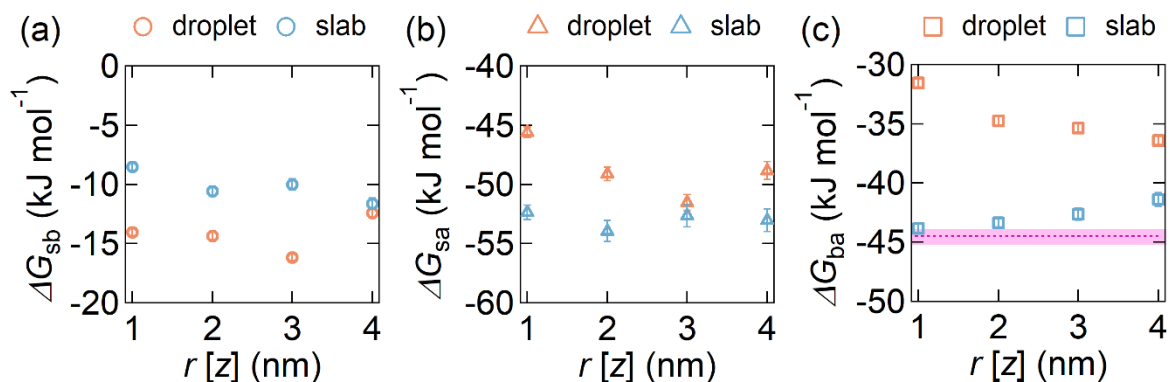
Figure 3: The differences of the free energy for succinic acid among the bulk, the surface and the air in different sizes of droplet (orange markers) and slab (blue markers) systems at 298.15 K. ΔG_{sb} (a), ΔG_{ba} (b), and ΔG_{sa} (c) are the free energy differences of the transition of the solute from the internal bulk volume to the liquid-vapor interface, the gas to the internal bulk volume of liquid, and the gas phase into the liquid-vapor interface, respectively. The pink block in (c) represent the free energy of hydration of succinic acid in bulk solutions ΔG_{hyd} by TI method calculation based on GAFF with ESP force field for succinic acid and TIP4P/2005 force field for water molecules (Fig. S1 and SI).

400
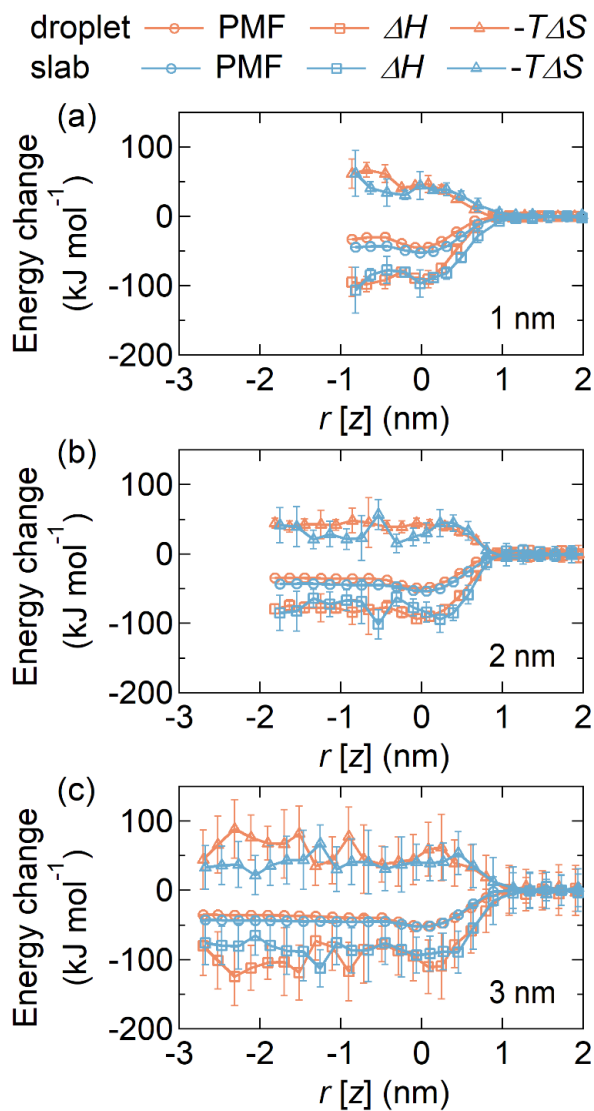
Figure 4: Decomposition of the potential of mean forces into enthalpic components and entropic components with different sizes in the droplet (radius) and slab (half slab thickness) systems. The lines with open circles represent the PMF profiles, the lines with open rectangles represent the enthalpic components (ΔH), and the lines with open triangles represent the entropic components ($-T\Delta S$).
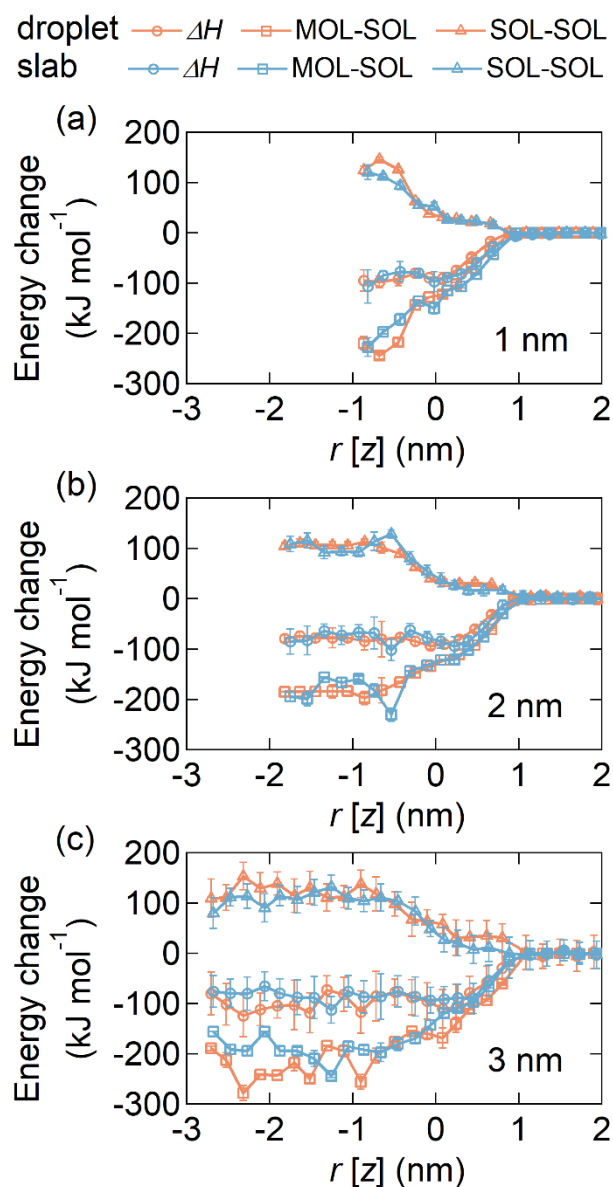
Figure 5: Decomposition of the enthalpic component into succinic acid-water and water-water interactions with different sizes in the droplet (radius) and slab (half slab thickness) systems. The lines with open circles represent the enthalpic components (ΔH), the lines with open rectangles represent the succinic acid-water interactions (MOL-SOL), and the lines with open triangles represent the water-water interactions (SOL-SOL).
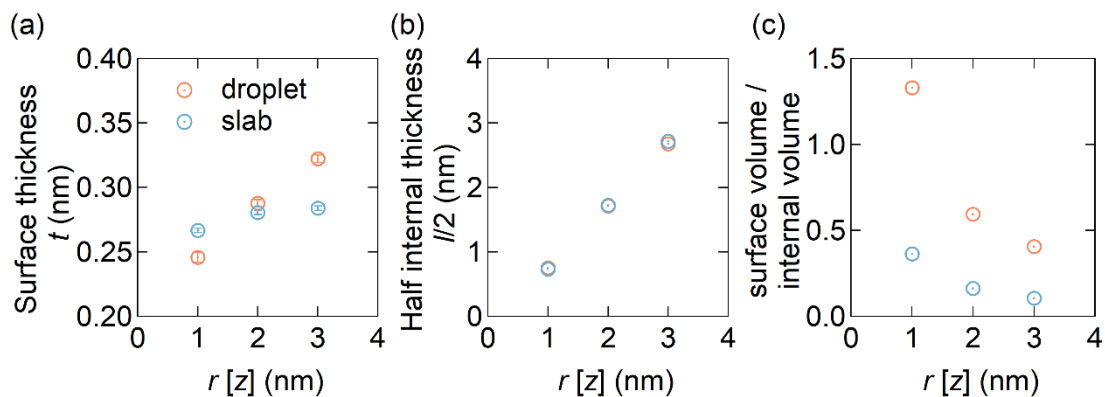
Figure 6: Structures of the droplet and slab systems with different sizes at 298.15 K. (a). Surface thicknesses of the droplet and slab systems. (b). Half internal thicknesses of the droplet and slab systems. (c). Ratio of surface volume versus internal bulk volume of the droplet and slab systems.

415